Microchimica Acta (2020) 187:621
https://doi.org/10.1007/s00604-020-04596-x

ORIGINAL PAPER

A paper-based colorimetric sensor array for discrimination and simultaneous determination of organophosphate and carbamate pesticides in tap water, apple juice, and rice

Mohammad Mahdi Bordbar[1] · Tien Anh Nguyen[2] · Fabiana Arduini[3] · Hasan Bagheri[1]

Received: 21 August 2020 / Accepted: 7 October 2020

Abstract

A colorimetric paper-based sensor is proposed for the rapid monitoring of six major organophosphate and carbamate pesticides. The assay was constructed by dropping gold and silver nanoparticles on the hydrophilic zones of a paper substrate. The nanoparticles were modified by L-arginine, quercetin, and polyglutamic acid. The mechanism of sensing is based on the interaction between the pesticide and the nanoparticles. The color of nanoparticles changed during the interactions. A digital camera recorded these changes. The assay provided a unique response for each studied pesticide. This method can determine six individual pesticides including carbaryl, paraoxon, parathion, malathion, diazinon, and chlorpyrifos. The limit of detection for these pesticides were 29.0, 22.0, 32.0, 17.0, 45.0, and 36.0 ng mL^{-1}, respectively. The assay was applied to simultaneously determine the six studied pesticides in a mixture using the partial least square method (PLS). The root mean square errors of prediction were 11, 8.7, 9.2, 10, 12, and 11 for carbaryl, paraoxon, parathion, malathion, diazinon, and chlorpyrifos, respectively. The paper-based device can differentiate two types of studied pesticide (organophosphate and carbamate) as well as two types of organophosphate structures (oxon and thion). Furthermore, this sensor showed high selectivity to the pesticides in the presence of other potential species (e.g., metal ions, anions, amino acids, sugar, and vitamins). This assay is capable of determining the pesticide compounds in tap water, apple juice, and rice samples.

Keywords Colorimetric detection · Paper-based device · Statistical multivariate analysis · Enzymeless sensors · Sensor array

Introduction

Among the different types of pesticides, organophosphates and carbamates are the most used compounds for eliminating insects and increasing the agricultural productivity [1]. However, the pesticide residue contaminates the soil and water, with severe environmental pollution level [1]. Furthermore, humans are affected by these compounds through inhalation, skin penetration, and contaminated food and water [2, 3]. These pesticides inhibit the acetylcholinesterase enzyme (AChE) activity resulting in neurological and respiratory disorders and even death [4]. Therefore, the monitoring of pesticides in food and environmental samples is a huge issue.

Chromatographic methods are the most commonly used analytical assays for the measurement of pesticides [5]. These methods have the desired requirements to analyze the trace amount of analytes encompassing high sensitivity, reproducibility, and accuracy [5]. Enzyme-linked immunosorbent assay (ELISA) is the other popular method based on an antigen's reaction, namely pesticides and antibody linked with enzyme [6]. Despite being highly sensitive, this method suffered from antibody usage, which requires animals [7].

Free enzyme optical sensor based on the lock-key principle provides a simple and inexpensive device in which the pesticides react with appropriate colorimetric receptors [8]. However, it shows disappointing results for the simultaneous

Electronic supplementary material The online version of this article (https://doi.org/10.1007/s00604-020-04596-x) contains supplementary material, which is available to authorized users.

✉ Hasan Bagheri
h.bagheri@bmsu.ac.ir; h.bagheri82@gmail.com

[1] Chemical Injuries Research Center, Systems Biology and Poisonings Institute, Baqiyatallah University of Medical Sciences, Tehran, Iran

[2] Department of Physics, Le Quy Don Technical University, Hanoi, Vietnam

[3] Department of Chemical Science and Technologies, University of Rome Tor Vergata, Via della Ricerca Scientifica, 00133 Rome, Italy

Published online: 21 October 2020

analysis of compounds with similar structures in the complex mixture [9].

To improve the selectivity, the array-based devices can be constructed by assembling a set of sensors that created a fingerprint pattern for a specified sample in the presence of other interferences [10]. Organic dyes, metal complexes, or nanoparticles can be used as sensing elements in the array structure. Nanoparticles (NPs) are sensitive sensing nanomaterials thanks to many properties such as high adsorption coefficient and the high surface-to-volume ratio [3, 11, 12]. A high adsorption coefficient happens because of the localized surface plasmon resonance (LSPR) which is the main properties of NPs [13]. This phenomenon occurs due to the interaction of the metal with incident electromagnetic radiation leading to the collective oscillation of conductive electrons at the interface of metal NPs [13]. The robustness of LSPR depends on various parameters such as size, shape, and composition of NPs as well as the interparticle distance between two individual NPs. The LSPR of NPs strongly affects the optical properties of metallic NPs [14, 15]. Among the various type of metallic NPs, gold (Au), silver (Ag), and copper (Cu) NPs show the high SPR absorption bands in the visible wavelengths. The respective prepared solution of these NPs has intense color [13]. Compared to CuNPs, both AuNPs and AgNPs are more attractive because of their unique properties such as high stability, biocompatibility, and versatility [16]. These advantages cause these NPs to show excellent analytical performance as chemical and biochemical sensors. NPs can be coated by stabilizing agents with different physical and chemical features contributing to various interactions (e.g., Van der Waals, covalent, or hydrogen bonding). The unique optical properties of NPs can change after being exposed to the analyte due to the aggregation or the characteristic surface changes [17].

Moreover, array structures' efficiency depends on the substrate utilized to perform and control the experiment [18]. Compared to various types of the substrate such as glass, silicon, plastic, and polymers [19–21], the device created by the paper is easily available, flexible, and easily customized with indicators, exploiting the porous structure of the paper to load the reagents before the analysis, working as substrate and reservoir, as well [22, 23]. Using biological recognition elements such as DNA and enzyme, the paper-based analytical devices (PADs) have shown the capability to determine with colorimetric detection the pesticides [24–29]. However, these assays are encountering the drawbacks of low storage stability due to the presence of the bioreceptors [30]. The use of inorganic materials including the quantum dots [31, 32], molecularly imprinted polymer [33], metal oxide [30], and NPs [3, 34], allowed to deliver paper-based sensor with improved storage stability.

Experimental

Chemicals and solution

The stabilizing agents including L-arginine, quercetin, and polyglutamic acid (PGA); the studied pesticides consisting of carbaryl, paraoxon, parathion, diazinon, chlorpyrifos, and malathion; and some materials such as cysteine, histidine, ascorbic acid, and lysine were obtained from Sigma-Aldrich (USA). Silver nitrate ($AgNO_3$), gold (III) chloride trihydrate ($HAuCl_4{\cdot}3H_2O$), sodium borohydride ($NaBH_4$), potassium nitrate (KNO_3), sodium nitrate ($NaNO_3$), calcium nitrate tetrahydrate ($Ca(NO_3)_2{\cdot}4H_2O$), magnesium nitrate hexahydrate ($Mg(NO_3)_2{\cdot}6H_2O$), sodium citrate, sodium sulfate (Na_2SO_4), sodium nitrate ($NaNO_3$), sodium sulfide (Na_2S), sodium cyanide (NaCN), ethanol, boric acid, and tris-hydroxymethyl methane (Tris) were purchased from Merck Chemical Company (Germany). D-Glucose and sucrose were purchased from Fluka. The sensor was fabricated on Whatman Grade No. 2 filter paper (Whatman LTD Company). The pesticide solutions (30 μg mL^{-1}) were initially prepared in ethanol and diluted to the desired concentrations with deionized water.

Apparatus

The data for the characterization of nanoparticles were collected by field emission scanning electron microscopy (FE-SEM; MIRA3 TESCAN) and SEM-attached energy-dispersive spectroscopy (EDX) (MIRA3 TESCAN). Transmission electron microscopy (TEM) was used to show the morphology of synthesized NPs (Philips, EM 208S). The designing patterns were drawn and printed on a paper substrate by AutoCAD 2016 software and an HP LaserJet printer 1320. The photos were taken by a Canon EOS 750D digital and were analyzed by Image J software (1.51n, National Institutes of Health, USA). MATLAB R2015 scientific software was applied for all statistical analysis.

Synthesis of studied NPs

The following experimental procedures were used to synthesize six studied NPs:

AgNPs functionalized by L-arginine $NaBH_4$ powder (0.01 g) was dissolved in 100.0 mL of deionized water. Then, 500.0 μL of the prepared solution was gradually mixed with 50.0 mL of silver nitrate solution (1.0×10^{-4} M) under stirring conditions. During this time, the solution turned yellow. After that, 1.0 mL of the aqueous solution of L-arginine (1.0×10^{-3} M) was added to 10.0 mL of unmodified AgNP solution to prepare L-arginine capped AgNPs. The excess amount of

amino acid was eliminated by centrifuging the prepared mixture [35].

AuNPs functionalized by L-arginine Under the stirring condition, the aqueous solution of 400.0 μL of $NaBH_4$ (2.5×10^{-4} M) was gradually added to the boiled $HAuCl_4$ solution (1×10^{-4} M) until the yellow color of the mixture changed to ruby-red. Then, 1.0 mL of L-arginine solution (1.0×10^{-3} M) was introduced to 10.0 mL of the previous mixture. The mixture's pH was adjusted at 7.0 by the addition of 30.0 μL of NaOH solution [36, 37].

AgNPs modified by quercetin Ethanolic solution of quercetin (800.0 μL) (1.0×10^{-3} M) was gradually added to 100.0 mL of $AgNO_3$ solution (1.0×10^{-3} M). The mixture was stirred vigorously. The experiment was continued until a stable yellow-brownish color appeared [38].

AuNPs modified by quercetin The alkaline solution of quercetin (0.5 mL) (2.0×10^{-3} M) was prepared an appropriate amount of the quercetin in (1.0×10^{-2} M) NaOH solution and immediately mixed with 10.0 mL of the aqueous solution of $HAuCl_4$ (1.0×10^{-3} M). The mixture was kept on the stirrer for 15 min. Over this time, the color of the solution turned to red [39].

AgNPs functionalized by PGA PGA (0.5 mL) (0.1 wt%) was transferred to a round-bottom flask containing 20.0 mL of deionized water, 0.5 mL of NaOH (0.5 M), and 10.0 mL of glucose (1% w/v). The mixture was stirred for 5 min. Then, the prepared solution was mixed with 0.5 mL of $AgNO_3$ (0.1% w/v). Forming AgNPs is accompanied by changing the solution's color from colorless to yellow color [40].

AuNPs functionalized by PGA First, 20.0 mL of the aqueous solution of $HAucl_4$ (5.0×10^{-2} M) was mixed with 10.0 mL of D-glucose solution (3.0×10^{-2} M). To this solution, 1.0 mL of PGA (0.1% w/v) was added. The reaction was completed by adding dropwise addition of NaOH (280.0 μL, 0.5 M). In this time, the red color of the solution was observed [40, 41].

After finishing the synthesis procedures, the prepared solution was centrifuged at 3900 rpm for 20 min to remove the free capping agents and free metal ions from the synthesized NPs. The residue was then re-dispersed in deionized water to form the NP solution.

Fabrication of paper-based sensor array

The PAD was fabricated by printing the proposed pattern (represented in Fig. 1a) on a paper substrate. The proposed pattern was drawn in AutoCAD software. Then, the paper was kept in the oven at 200 °C for 45 min. In this condition, the printer ink was penetrated the substrate texture, delivering suitable hydrophobic barriers [42]. The hydrophilic part consisted of six circular spots, and it was used for the detection and sampling zones. In detail, each spot was coated with 1.0 μL of selected sensing element constituted of NPs dissolved in buffer solution. The injection zone consists of a rectangular area that covers the whole of the detection zone. The image of the fabricated PAD-based sensor array is shown in Fig. 1.

Colorimetric analysis

For pesticide detection, the fabricated PAD was folded. The injection zone was placed on the detection part. Then, 10.0 μL of each pesticide was added to the sampling zone. This value was appropriate for effective and complete interaction between analyte and NPs. The analyte was homogeneously distributed on the surface of the paper and simultaneously interacted with NPs in different detection zones. The sensor images were collected after 15 s. To avoid the effect of ambient light during the image acquiring process, the photos were captured in the laboratory cabinet. For each sensing element, changes in the color of NPs were calculated using ImageJ software.

The software also converted the color intensity of each spot embedded in the PAD structure to three numerical mean values corresponding to red, green, and blue color elements. This experiment was performed for both PAD photos obtained before and after exposure to the pesticide. The difference between the color values of the before and after photos was calculated by the following equation:

$$\Delta R = \overline{R}_{after} - \overline{R}_{before}$$

$$\Delta G = \overline{G}_{after} - \overline{G}_{before}$$

$$\Delta B = \overline{B}_{after} - \overline{B}_{before}$$

In this equation, the difference values of red, green, and blue color elements were shown with ΔR, ΔG and ΔB, respectively. Finally, for six spots used in the array, the results were accumulated in a data vector with 18 members (3 RGB color elements for 6 different NPs) for each pesticide. Next, each spot's difference values were re-converted to color intensity to provide a color difference map. Five repetitive measurements were performed for each experiment. Scheme S1 presents a summary of the colorimetric procedure.

In the pesticide analysis, 30 response vectors were obtained for the 6 tested pesticides and were collected in a dataset with the size (30 × 18). This matrix was applied as an input of statistical methods such as principal component analysis (PCA), hierarchical cluster analysis (HCA), and linear discriminate analysis (LDA) to find the discriminatory ability of PAD.

As such, PAD was used to determine the different amounts of individual pesticide (0.1 ng mL^{-1} to 30 μg mL^{-1}). For each

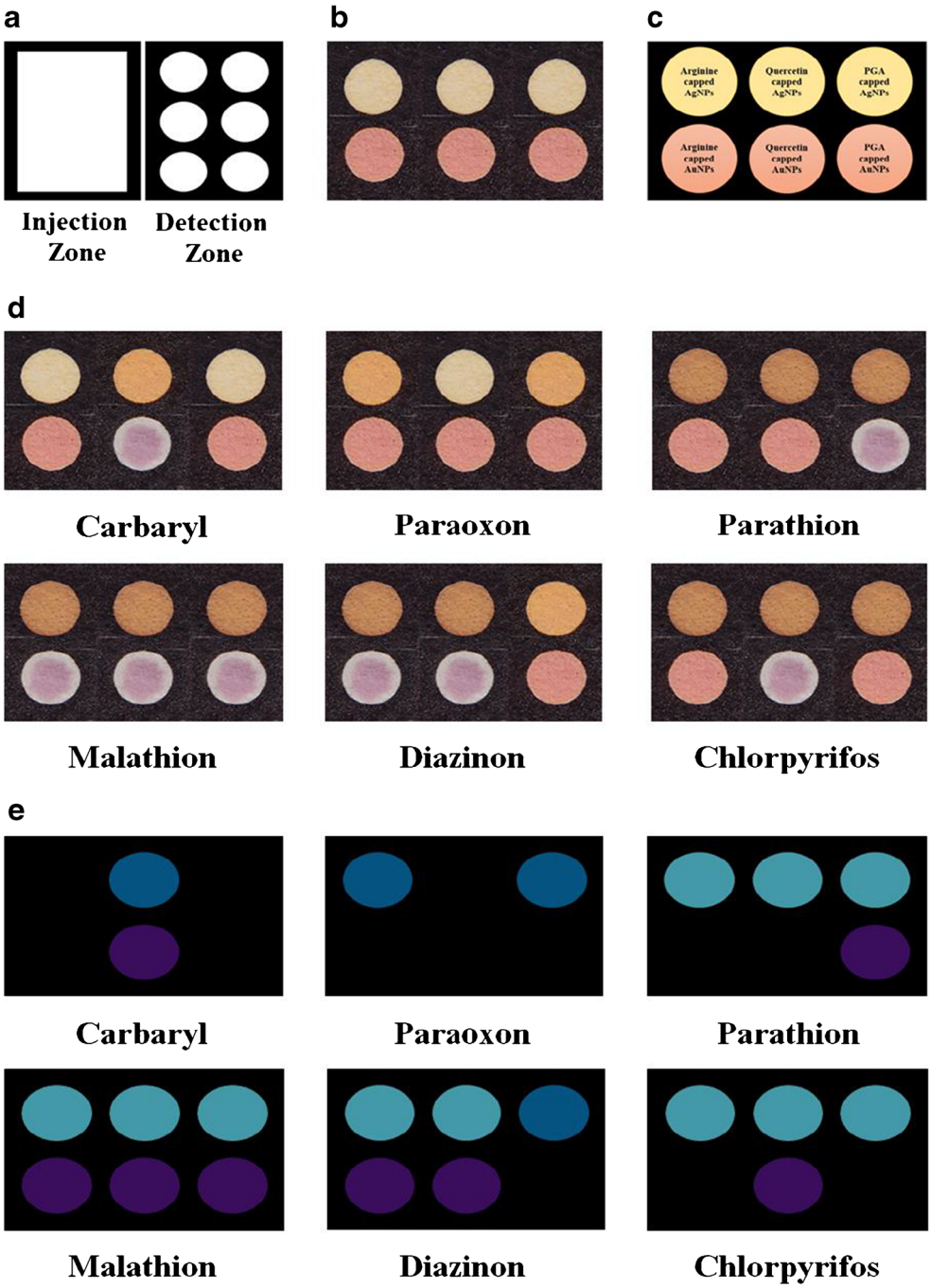

Fig. 1 **a** The schematic of designing PAD. **b** The image of the fabricated sensor array. **c** A pattern for the introduction of sensing elements. **d** Response of sensor and **e** color profiles for 6 different types of pesticides (1.0 μg mL^{-1}). The experiment was done at optimized conditions (Tris buffer (0.5 μL, 0.10 M, pH = 9.0) and 0.35 μL of NPs). The response of the sensor was captured after 15-s incubation

determination, the Euclidean norm of the response vector was calculated as the response of the sensor array. These values were plotted against the different concentrations to obtain the calibration curve.

For quantitative analysis, the simultaneous determination of 6 pesticides was studied using a training set containing twenty standard mixtures. Each mixture was provided according to a regular guideline [43], summarized in Table S1. The developed sensor analyzed the standard solutions. The collected data with the size of (20 × 18) was subjected to the partial least squares (PLS) method to fabricate a mathematical model. A prediction set including five standard mixtures (Table S1) was used to evaluate the resulting model.

Real sample analysis

In this study, tap water, apple, and rice samples were selected as matrices to demonstrate the ability of the sensor to detect the pesticides in real samples. In detail, five different solutions were prepared by mixing six pesticides at different concentrations. All samples were individually spiked with each mixture. For apple and rice, 20.0 g of the contaminated samples were

crushed fine and added to 25.0 mL of methanol. After sonication, the mixture was filtered using syringe filters (0.22 μm) 3 times [44]. The solution was used for further studies. The spiked water samples were analyzed without any pretreatment. Then, the fabricated PAD was exposed to 10.0 μL of each real sample. The obtained results were investigated by the PLS calibration model to find the concentration of each pesticide in the studied samples.

Results and discussion

In this study, the performance of a paper-based colorimetric sensor array was evaluated to detect different types of pesticides. The array is composed of AuNPs and AgNPs, which are synthesized with non-enzyme capping agents. These NPs show an absorbance peak in the visible wavelength region, being appropriate for colorimetric detection. These NPs indicate different responses to various types of pesticides, thanks to the different interactions in the chemical structure of capping agents and analytes. The best interaction is obtained at optimized conditions. Besides discrimination, the sensitivity of the sensor was investigated in both individual and simultaneous determination of six studied pesticides.

Characterization

Standard analytical methods characterized the processes of nanoparticles preparation and sensor fabrication. The morphology of prepared NPs was verified by TEM. Figure 2 indicates that all NP were monodispersed and synthesized in a spherical shape. The size distribution histograms obtained by dynamic light scattering (DLS) measurements were applied to estimate the hydrodynamic diameter of synthesized NPs. The bar plots shown in the inset of each TEM image reveal that the size of NPs was normally distributed around 28, 40, and 36 nm for AgNPs modified by arginine, quercetin, and PGA, respectively. The respective values for AuNPs are equal to 20 nm, 20 nm, and 24 nm. The absorption spectra of synthesized NPs (Fig. S2) indicate a unique plasmon resonance peak at 410 nm for arginine capped AgNPs, 525 nm for arginine capped AuNPs, 430 nm for quercetin capped AgNPs, 520 nm for quercetin capped AuNPs, 405 nm for PGA capped AgNPs, and 530 nm for PGA capped AuNPs. In these wavelengths, the respective absorbance intensities of each employed NPs were achieved as 1.11, 1.10, and 0.69 for AgNPs and 0.63, 1.19, and 0.59 for AuNPs modified by arginine, quercitin, and PGA, respectively.

Figure S3 shows the FT-IR spectra of the free modifier and the respective synthesized NPs. The similarity in several particular IR bonds demonstrates that these materials successfully functionalized the NPs. The description of the FT-IR spectra of each synthesized NPs was represented in supporting information document (Section 1).

The SEM images of the fabricated sensor are shown in Fig. S4. This figure illustrated the structure of bare filter paper and hydrophobic barrier and the distribution of synthesized NPs on the surface of hydrophilic zones. Also, Fig. S5 shows the EDX spectra of arginine capped AgNPs and AuNPs with the strong peaks located at 3 keV and 2.3 keV, respectively. It is used to confirm the presence of silver and gold elements in the synthesized NPs.

The additional information about these experiments was represented in supporting information (Section 1–2). Also, the relevant plots are reported in Fig. S2-S5 and Table S2.

Repeatability and stability

To ensure that the sensor manufacturing process is repeatable, five PADs were individually fabricated. The color intensity of each sensing element was calculated in RGB values and the relative standard deviation (RSD) was measured for each color element. As shown in Table S3, the RSD % of the red, green, and blue color elements are respectively equal to 1.03, 1.05, and 1.18 for L-arginine capped AgNPs; 0.89, 0.93, and 1.03 for L-arginine capped AuNPs; 0.39, 0.68, and 0.98 for quercetin capped AgNPs; 0.40, 0.82, and 1.04 for quercetin capped AuNPs; 0.70, 1.14, and 0.96 for PGA capped AgNPs; and 0.84, 0.93, and 1.19 for PGA capped AuNPs. As seen, the RSD amounts are lower than 10% for each color element, indicating no significant difference was observed between the color values. Therefore, the sensor was prepared by a repeatable procedure.

The lifetime of the sensor was evaluated by monitoring the color values of each sensing element for a period of time. As illustrated in Fig. S6, no color changes were observed for 1 month. After this time, the sensor cannot tolerate physical or chemical variations.

Optimization

The assay responses to studied pesticides can be influenced by some effective parameters such as the volume of NPs, pH, type, and concentration of buffer solution. These parameters should be optimized to find the maximum responses of the sensor for each analyte. Discrimination ability function (DAF) [43] was used to find the best conditions. The definition of this equation is given in supporting information (Section 3). The maximum amount of DAF was selected as the optimum value for each parameter.

For the first experiment, a different volume of NPs (0.1 to 0.5 μL) was used to interact with the selected pesticides. As shown in Fig. S7a, the best interaction was observed when the volume of NPs was 0.35 μL. Therefore, 0.5 μL of buffer solution and 0.35 μL of NPs were mixed. The results were

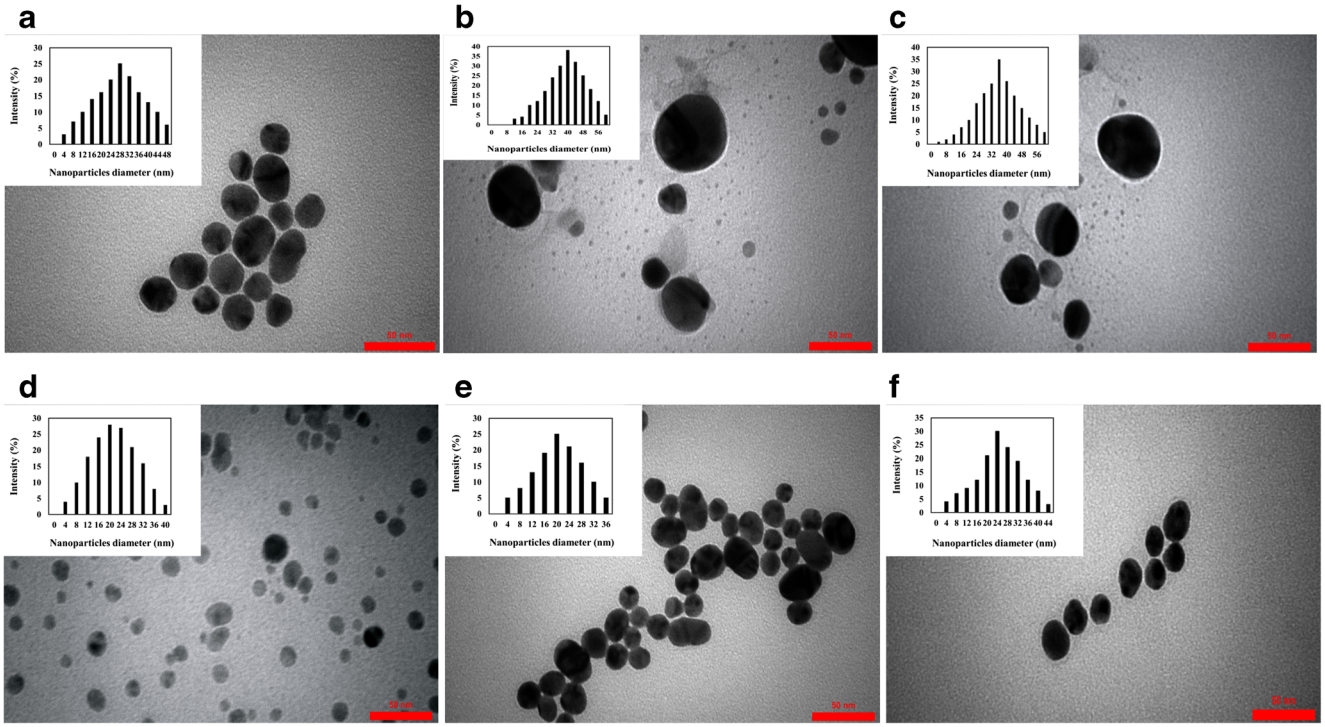

Fig. 2 The TEM images and hydrodynamic size histograms of synthesized NPs. **a** L-Arginine capped AgNPs. **b** Quercetin capped AgNPs. **c** PGA capped AgNPs. **d** L-Arginine capped AuNPs. **e** Quercetin capped AuNPs. **f** PGA capped AuNPs

not suitable at higher volumes because the sensing elements have intense color and prevent the minor changes obtained by the interaction of analytes and NPs.

The volume of the mixture was adjusted to 1.0 μL by adding 0.15 μL of deionized water. This mixture was applied to fabricate each sensing element for further study.

The interaction of NPs and pesticides was investigated at different pH levels in the range of 3.0 to 11.0. As illustrated in Fig. S7b, the higher DAF value was achieved at pH 9.0 for all studied NPs. The weak interactions occurred in acidic and strong alkaline media due to the protonation of functional groups and electrostatic repulsions, respectively.

Also, the response of the sensor was monitored in two different types of buffer solution (Tris and borate) at an optimal pH. Using the Tris buffer in the sensing element matrix, the suitable responses were observed (Fig. S7c). Therefore, this buffer was selected for further study.

The buffer concentration is the last critical factor investigated in this study. As seen in Fig. S7d, the DAF value gradually increased by changing the concentration of the buffer solution from 0.02 to 0.10. At higher concentrations, the response of the sensor was decreased clearly because of ionic interferences.

Assay observations

The colorimetric responses of the sensor to six studied pesticides were presented in Fig. 1d. As seen, the interaction of sensing elements with a specified pesticide causes the aggregation of NPs. Therefore, the color of the sensor changed from red to purple for AuNPs or from pale yellow to brown for AgNPs. These changes depend on the strength of bonding between NPs and analytes. Each NP covers by a specified capping agent and the used capping agent possesses various functional groups in its structure. For example, arginine and PGA contain amino and carboxyl groups, while quercetin includes hydroxyl and carbonyl groups in their structure. These functional groups participate in the H-bonding interactions with the analytes, categorized in hydrogen donating or hydrogen accepting materials or none of them.

On the other hand, the electrical charge on the surface of NPs and analytes can be different. One material is more positive, and the other is more negative; therefore, they can interact together through electrostatic interaction. Also, the capping agents varied in size. Arginine is smaller molecules so that it can interact with most of the analytes. However, PGA is a polymer compound and occupies more space around the central core [45]. Therefore, a big-sized analyte cannot interact with this capping agent because of steric hindrance. Capping agents can be involved in the electrophilic or nucleophilic interactions because of the high affinity of phosphor atom to form P-N, P-O, or P-S bonds [46, 47]. Finally, a typical analyte can take part in H-bonding, electrostatic or nucleophilic interaction (maybe all of them) based on its structural chemistry. So, it can show different behavior toward six studied NPs. The aggregation of NPs after interaction with

pesticides was confirmed by SEM images given in Fig. S8. It is schematically shown in Scheme S2.

As shown in Fig. 1d, malathion has high interest in interaction with all sensing elements because of various active sites in its chemical structure. AgNPs synthesized by arginine and PGA can discriminate between carbamic pesticide and organophosphorus compounds. These NPs aggregated in the presence of phosphor-containing materials which resulted in appearing in the deep brown color. However, paraoxon has a weak interaction with these NPs. It can only increase the color intensity of the sensing element to intense yellow. Probably, these NPs have a high affinity to sulfur-containing compounds, while paraoxon has no sulfur atom in its chemical structure. The similar response was obtained for the reaction of diazinon and PGA-AgNPs due to the interferences of methyl groups in the analyte structure. The quercetin-AgNPs can be used to differentiate between two classes of organophosphate pesticides (thion and axon). It tended to interact with thio-based organophosphates while showing no responses to oxon compounds. These NPs have strong interaction with carbaryl through hydrogen bonding between nitrogen atom in carbaryl structure and hydroxyl groups of quercetin. The quercetin-AuNPs can identify the amino-containing pesticides (carbaryl, diazinon, and chlorpyrifos). These NPs and PAG-AuNPs create a difference between thions with amino substituent and parathion pesticide. In the end, arginine-AuNPs can be introduced as an appropriate sensing element for detecting diazinon in the presence of the other organophosphorus pesticide, chlorpyrifos.

The absorption spectra of each synthesized NPs after interaction with studied pesticides are shown in Fig. S9. As shown in this figure, each NPs have a different tendency to different types of pesticides. The location of the maximum wavelength did not change when the NPs have no interaction with pesticides. On the other hand, a redshift was observed in the absorption spectrum after the aggregation of NPs in the presence of pesticides.

Changes in the color of the proposed sensor are represented in a format of colorimetric profiles (Fig. 1e). Each profile is considered as an identity card for each studied pesticide comprising the important data about the name, type, chemical structure, and also physiochemical properties. The difference maps confirmed all observations obtained by visual detection. However, the minor changes in the color of NPs are well exhibited in this figure. For example, the difference between the color of arginine-AgNPs in the presence of oxon and thion pesticides was clearly elucidated. Also, the map of PGA-AgNPs indicated the less color intensities for paraoxon or diazinon rather than the other organophosphates.

Analytical features

The proposed array was individually exposed to different concentrations of each studied pesticides. For this purpose, the solution of the pesticide compound was prepared with the concentration in the range of 0.0 to 30.0 μg mL^{-1}. Then, 10.0 μL of each prepared solution was added to the injection zone. The complete interaction was achieved after 15 s. After this time, the color changes in the detection zone were monitored by a camera. After image processing, each concentration's colorimetric difference map was obtained and represented in Fig. 3. As observed in this figure, the changes in the color of sensing elements were correlated with the concentration of pesticides. By increasing the concentration, the color intensity of each spot embedded in the colorimetric map was raised. Also, the calibration curve was drawn by plotting the Euclidean norm of the response vector of each concentration against the concentrations of pesticides. Figure 4 indicates that the relationship between the response of assay and the amount of pesticide was linear in the range of 35.0 ng mL^{-1}–2.5 μg mL^{-1} for carbaryl, 25.0 ng mL^{-1}–5.0 μg mL^{-1} for paraoxon, 35.0 ng mL^{-1}–5.0 μg mL^{-1} for parathion, 20.0 ng mL^{-1}–2.5 μg mL^{-1} for malathion, 50.0 ng mL^{-1}–7.5 μg mL^{-1} for diazinon, and 40.0 ng mL^{-1}–2.5 μg mL^{-1} for chlorpyrifos. The limits of detection for these determinations are represented in Table 1 which are equal to 29.0, 22.5, 32.5, 16.7, 44.6, and 36.1 ng mL^{-1} pertinent to carbaryl, paraoxon, parathion, malathion, diazinon, and chlorpyrifos, respectively. The detection limit was obtained according to the $3\sigma/m$ criterion (where σ is the standard deviation of the blank or standard deviation of the intercept and m is the slope of the calibration plot).

Discrimination analysis

The efficiency of the sensor for discrimination of pesticides was statistically verified using some recognition methods such as PCA and HCA. PCA converts the raw data matrix into two individual matrices which are defined as score (T) and loading (L) matrices. The new data in the score matrix was sorted according to reducing the variances. Therefore, the first columns of this matrix (which are called as principle component) include the highest explained variances and minimum noisy data. The first principle components (PCs) can be used for further visualization and determination analysis. The PCA score plot shown in Fig. 5a was obtained by plotting the second PC versus the first PC. This figure shows that 92% of the important information (explained variances) were distributed in the space of two first PCs. As it was clear, six individual pesticides were well separated and classified into two organophosphate and carbamate families. The sulfur-containing pesticides were completely discriminated from the other analytes. Also, a proper dissociation was observed between the pesticides comprising amino groups and the other thion materials. The first PC can differentiate between the compounds with aromatic and aliphatic pesticides.

According to HCA dendrograms, the studied pesticides were divided into 3 clusters: carbamates, axons, and thions. As shown in Fig. 5b, each cluster includes the relevant analytes and no misclassification was observed in this study.

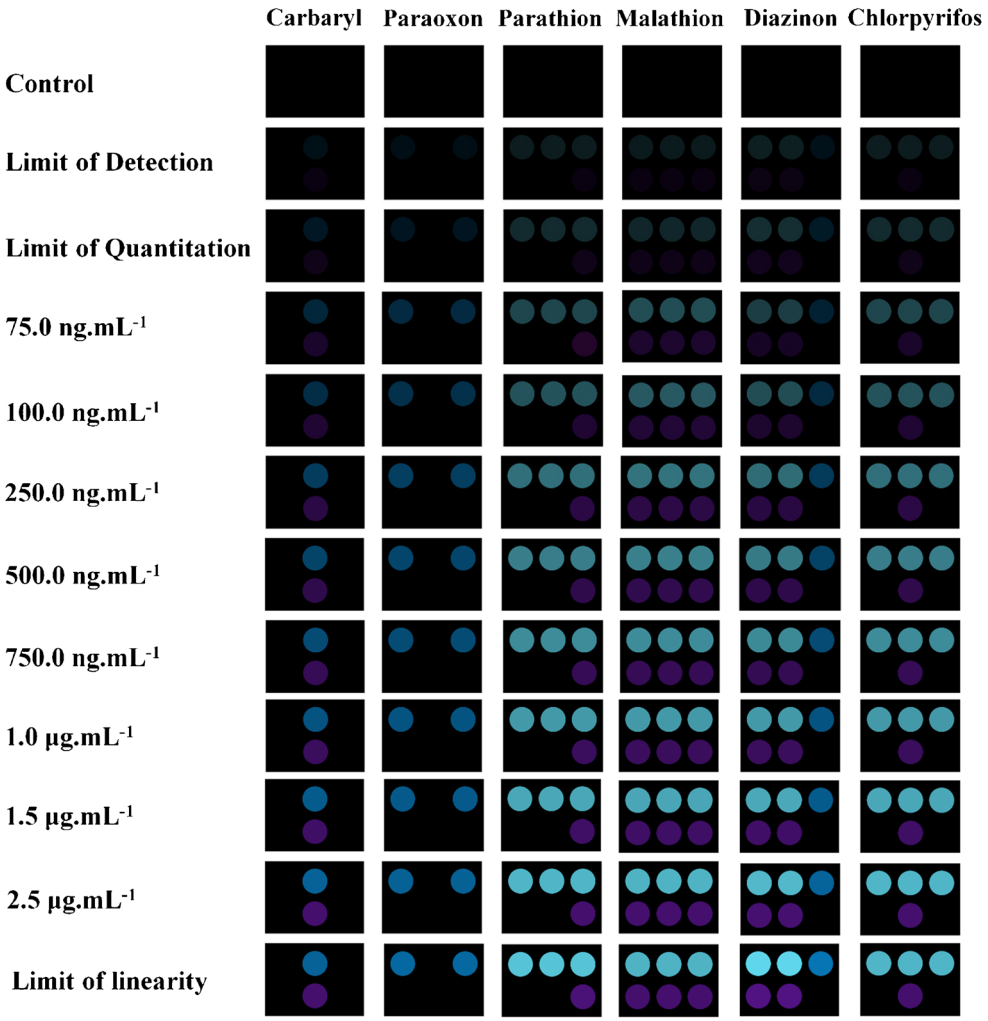

Fig. 3 The colorimetric profiles of the sensor in the presence of pesticides at different concentrations

Also, the ability of the sensor was examined by LDA. Therefore, the response was distributed into a training set to propose the LDA model and a prediction set to investigate the model proficiency. Figure S10 demonstrates that the developed model is reliable to predict the unknown sample with high accuracy. Also, the discrimination results obtained by this method are more acceptable than the previous analyses. Two first LDA factors can clearly differentiate between carbamate and organophosphates, axon and thions.

HCA methods evaluated the discrimination analysis of the pesticides at the other concentrations. For this study, the pesticide was used with the following concentrations: 75.0 μg mL^{-1}, 100.0 μg mL^{-1}, 250.0 μg mL^{-1}, and 500.0 μg mL^{-1}. The HCA dendrograms, presented in Fig. S11, confirm that the developed sensor created a clear difference between individual pesticides as well as their categories at very low concentrations.

Analysis of pesticide mixtures

The PLS regression method was applied to verify the potential of the sensor to determine six studied pesticides in a mixture. The mixing solutions for training and validating the PLS model are represented in Table S1. The mathematical model was run via effective numbers of latent variables obtaining by the leave-one-out cross-validation (LOO-CV) method. The accuracy of the model was evaluated by calculating the root mean square errors (RMSE) for both calibration and prediction sets. As shown in Table 2, the PLS method provided low error values meaning that the model is acceptable to find the concentration of pesticides in a sample with high accuracy. Also, Fig. 6 indicates the high correlation between the real concentrations of analytes and those obtained by the developed model. The obtained coefficients of determination (R^2) are included in Table 2. The results confirm that the model is highly reliable to determine the unknown sample concentration.

Study of selectivity

In addition to pesticides, the sensor was individually exposed to 25 μg mL^{-1} of the potential interferences including K^+, Na^+, Ca^{2+}, Mg^{2+}, SO_4^{2-}, NO_3^-, I^-, Br^-, Cl^-, S^{2-}, CN^-, cysteine, histidine, lysine, ascorbic acid, glucose and sucrose,

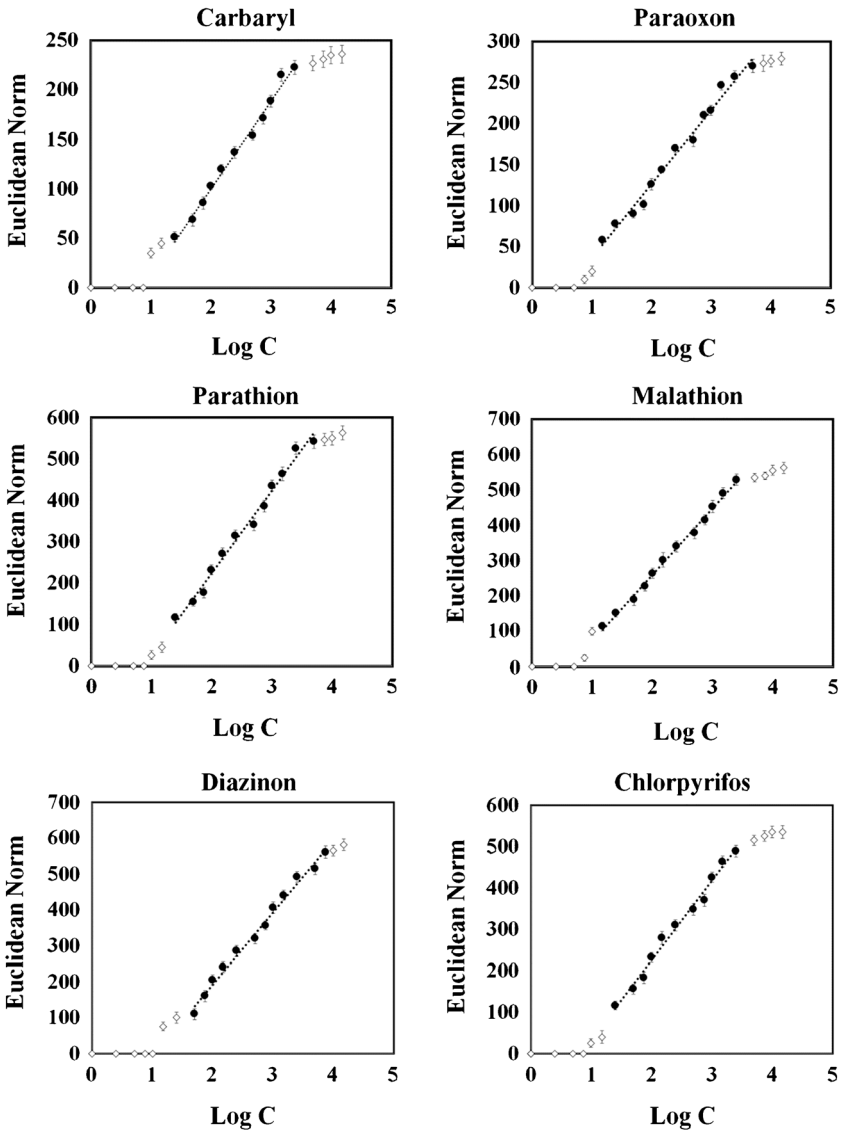

Fig. 4 Discrimination results obtained by **a** PCA and **b** HCA. The concentration of pesticides is equal to 1.0 μg mL^{-1}. The experiment was done under optimum condition (Tris buffer (0.5 μL, 0.10 M, pH = 9.0) and 0.35 μL of NPs). The response of the sensor was captured after 15-s incubation

methoxychlor, perthane, mirex, toxaphene, trichlorfon, tebuconazole, propiconazole, and chlorothalonil. The results were demonstrated in colorimetric maps (Fig. S12) and then analyzed by HCA in Fig. S13. For clarification, the responses to these materials were entirely distanced from those obtained by pesticides. Therefore, the proposed sensor provides a specific pattern for each studied pesticide. Interestingly, this sensor has a high performance for the distinction between various types of chemicals such as cations, anions, vitamins, amino acids, and sugars besides pesticides. In the next experiment, the probe was applied to analyze the mixture of each interfering species (with different concentrations) and 1 μg mL^{-1} of each studied analytes. As illustrated in Table S4, the sensor responses to pesticides were not affected by the foreign materials while their concentration was 25-, 50-, or 100-fold of analyte concentration.

Table 1 The analytical results for quantitative analysis of studied pesticides

Analyte	Linear range	Detection limit (ng mL^{-1})	R^2
Carbaryl	35.0 ng mL^{-1}–2.5 μg mL^{-1}	29.0	0.990
Paraoxon	25.0 ng mL^{-1}–5.0 μg mL^{-1}	22.0	0.986
Parathion	35.0 ng mL^{-1}–5.0 μg mL^{-1}	32.0	0.987
Malathion	20.0 ng mL^{-1}–2.5 μg mL^{-1}	17.0	0.992
Diazinon	50.0 ng mL^{-1}–7.5 μg mL^{-1}	45.0	0.985
Chlorpyrifos	40.0 ng mL^{-1}–2.5 μg mL^{-1}	36.0	0.988

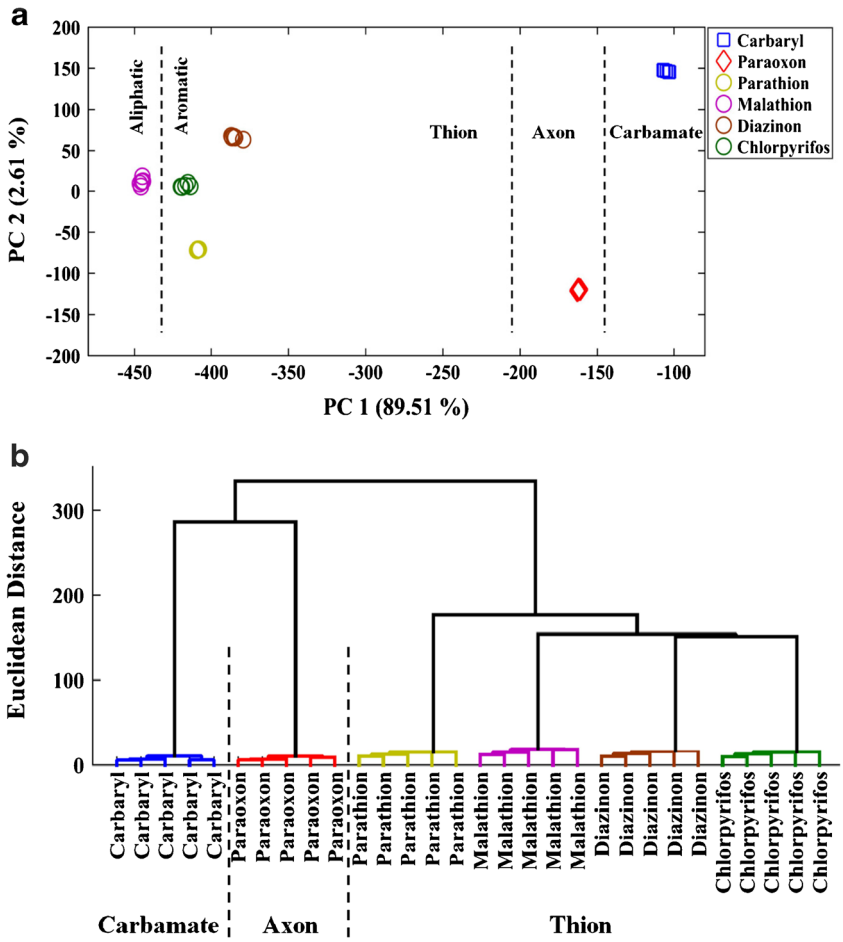

Fig. 5 The assay responses in the presence of studied pesticides at different concentrations. The concentration changed from 0.2 ng mL^{-1} to 30.0 μg mL^{-1}. The linear range is shown with the solid black circles. The experiment was done at optimized conditions (Tris buffer (0.5 μL, 0.10 M, pH = 9.0) and 0.35 μL of NPs). The response of the sensor was captured after 15 s incubation

Reproducibility of assay responses

To evaluate the reproducibility of the sensor, each pesticide (1 μg mL^{-1}) was examined for 5 times and the RSD for the results was calculated. As shown in Table S5, the RSD % values for five repetitive determinations of carbaryl, paraoxon, parathion, malathion, diazinon and chlorpyrifos are equal to 5.15, 4.44, 3.85, 5.95, 5.37, and 5.91, respectively. The amounts of RSD are lower than 10% for each measurement, confirming that the array provided the reproducible responses for each analyte.

Table 2 The statistical information obtained by PLS regression models

Analyte	PLS factor	RMSEC	RMSEP	R^2_C	R^2_P
Carbaryl	6	12	11	0.973	0.975
Paraoxon	7	10	8.7	0.975	0.978
Parathion	7	9.4	9.2	0.974	0.974
Malathion	6	12	9.6	0.977	0.981
Diazinon	7	15	12	0.978	0.979
Chlorpyrifos	7	10	11	0.975	0.975

Pesticide analysis in real samples

To monitor the capability of the assay for detecting pesticides in real samples, including tap water, apple and rice were contaminated with mixtures of six studied pesticides. The content of each mixture was summarized in Table S6. The colorimetric method and the developed PLS model estimated the amount of each pesticide were analyzed by the studied samples. As reported in Table S6, no pesticides were detected in the real samples before contamination. Also, the appropriate recovery values (93–107%) were obtained for the spiked materials. The results affirm that the proposed sensor is highly efficient for detecting pesticides in both environmental and food samples.

Finally, Table S7 illustrates that the analytical performance of the assay was comparable to previous reports. The prior methods based on enzymatic reactions were highly sensitive, but they did not produce a selective (or specific) responses to individual pesticides. They responded to various types of organophosphates or carbamates, which is an important challenge for these methods, especially when the different pesticides simultaneously existed in real samples. Also, these assay used an enzyme which increased the cost and time of

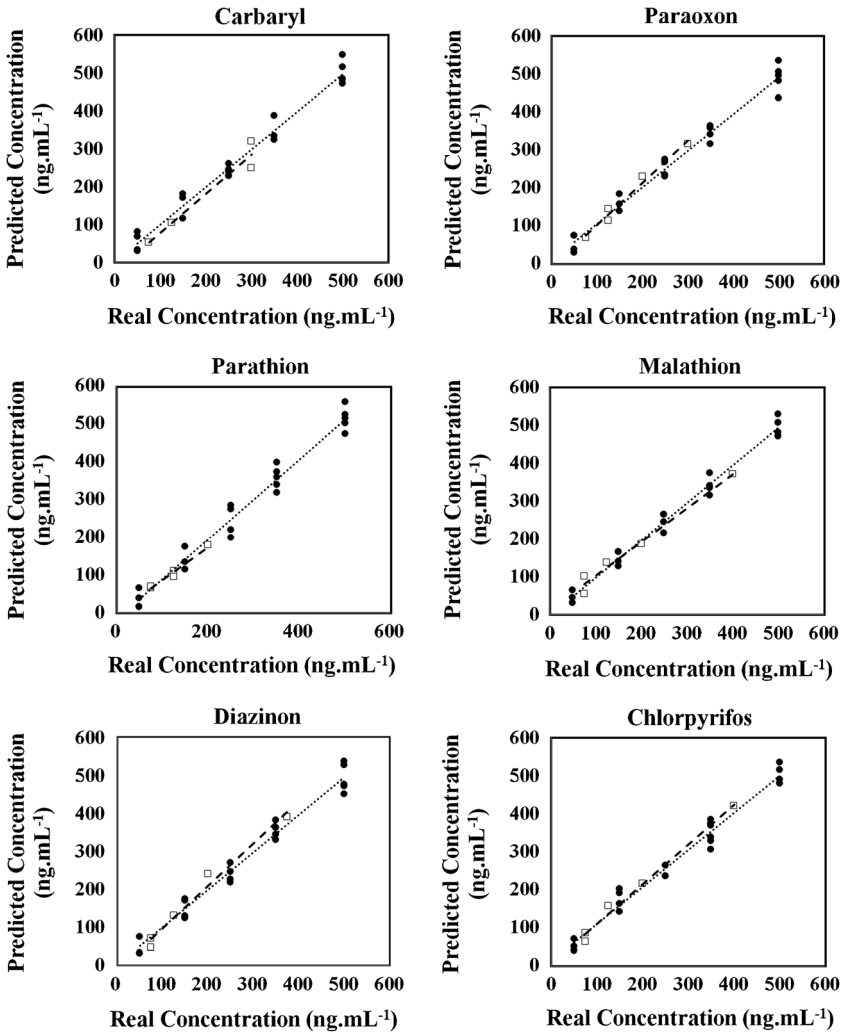

Fig. 6 The results were obtained by the PLS models for the simultaneous analysis of the studied pesticides. Solid circles and square markers were used to assign the training and test datasets, respectively. The experiment was done at the optimized condition (Tris buffer (0.5 μL, 0.10 M, pH = 9.0) and 0.35 μL of NPs). The response of the sensor was captured after 15-s incubation

treatment. The other methods utilize toxic materials as sensing elements that are not safe for the environment and humans. Compared to these assays, our work described 3D origami paper based optoelectronic tongue for detection of pesticide. This designing pattern help to prevent the coffee effect and to leach the sensing reagents. Therefore, it does not require to use stabilizers for immobilizing the reagents on the paper. Also, most of the responses are not wasted. In this work, we used nanoparticles which are synthesized by organic compounds and without needing enzyme, antibody or DNA. These NPs have antibacterial properties and safe. They were produced through an inexpensive and low-cost method and the assay preparation was not time-consuming. This assay was fabricated based on the colorimetric sensor array technology; therefore, it provided a specific response for each type of pesticide. It can also simultaneously determine the various type of pesticides in the real sample without any preparation methods to remove the foreign species. It can result that our proposed method can solve the drawbacks of the previous methods.

Conclusion

A new colorimetric probe was developed using the paper-based optical sensor array strategy. The detection principle is based on the aggregating AgNPs that are synthesized with different inexpensive chemical compounds and observing the color changes of sensing elements. The sensor has a high potential to clearly discriminate between different types of pesticides and distinguish them from the other foreign species. The assay indicated a sensitive, reproducible, and reliable responses for quantitative analysis of analytes in both individual and mixture samples. Due to the simplicity in the fabrication of PAD and rapidity in the detection, the probe can be applied as a cost-effective and available method to monitor pesticides in the real samples. However, the proposed method has some limitations: the detection mechanism is irreversible, the assay requires time for extraction of pesticide from real samples and it is not stable for more than a month.

Funding This study is financially supported by the Research Councils of Baqiyatallah University of Medical Sciences.

Compliance with ethical standards

Conflict of interest The authors declare that they have no competing of interests.

References

1. Pundir CS, Malik A, Preety (2019) Bio-sensing of organophosphorus pesticides: a review. Biosens Bioelectron 140:111348. https://doi.org/10.1016/j.bios.2019.111348
2. Xu ML, Gao Y, Han XX, Zhao B (2017) Detection of pesticide residues in food using surface-enhanced Raman spectroscopy: a review. J Agric Food Chem 65:6719–6726. https://doi.org/10.1021/acs.jafc.7b02504
3. Bordbar MM, Nguyen T-A, Tran AQ, Bagheri H (2020) Optoelectronic nose based on an origami paper sensor for selective detection of pesticide aerosols. Sci Rep. 10: 17302. https://doi.org/10.1038/s41598-020-74509-8
4. Grimalt S, Dehouck P (2016) Review of analytical methods for the determination of pesticide residues in grapes. J Chromatogr A 1433:1–23. https://doi.org/10.1016/j.chroma.2015.12.076
5. Souza Tette PA, Guidi LR, De Abreu Glória MB, Fernandes C (2016) Pesticides in honey: a review on chromatographic analytical methods. Talanta 149:124–141. https://doi.org/10.1016/j.talanta.2015.11.045
6. Songa EA, Okonkwo JO (2016) Recent approaches to improving selectivity and sensitivity of enzyme-based biosensors for organophosphorus pesticides: a review. Talanta 155:289–304. https://doi.org/10.1016/j.talanta.2016.04.046
7. Van Dyk JS, Pletschke B (2011) Review on the use of enzymes for the detection of organochlorine, organophosphate and carbamate pesticides in the environment. Chemosphere 82:291–307. https://doi.org/10.1016/j.chemosphere.2010.10.033
8. Yan X, Li H, Su X (2018) Review of optical sensors for pesticides. TrAC - Trends Anal Chem 103:1–20. https://doi.org/10.1016/j.trac.2018.03.004
9. Zhao M, Yu H, He Y (2019) A dynamic multichannel colorimetric sensor array for highly effective discrimination of ten explosives. Sensors Actuators B Chem 283:329–333. https://doi.org/10.1016/j.snb.2018.12.061
10. Bordbar MM, Hemmateenejad B, Tashkhourian J, Nami-Ana SF (2018) An optoelectronic tongue based on an array of gold and silver nanoparticles for analysis of natural, synthetic and biological antioxidants. Microchim Acta 185: https://doi.org/10.1007/s00604-018-3021-1
11. Khoshfetrat SM, Bagheri H, Mehrgardi MA (2018) Visual electrochemiluminescence biosensing of aflatoxin M1 based on luminol-functionalized, silver nanoparticle-decorated graphene oxide. Biosens Bioelectron 100:382–388. https://doi.org/10.1016/j.bios.2017.09.035
12. Bordbar MM, Tashkhourian J, Hemmateenejad B (2019) Structural elucidation and ultrasensitive analyses of volatile organic compounds by paper-based nano-optoelectronic noses. ACS Sensors 4:1442–1451. https://doi.org/10.1021/acssensors.9b00680
13. Zarlaida F, Adlim M (2017) Gold and silver nanoparticles and indicator dyes as active agents in colorimetric spot and strip tests for mercury(II) ions: a review. Microchim Acta 184:45–58. https://doi.org/10.1007/s00604-016-1967-4
14. Della Pelle F, Scroccarello A, Scarano S, Compagnone D (2019) Silver nanoparticles-based plasmonic assay for the determination of sugar content in food matrices. Anal Chim Acta 1051:129–137. https://doi.org/10.1016/j.aca.2018.11.015
15. Della Pelle F, Scroccarello A, Sergi M, Mascini M, del Carlo M, Compagnone D (2018) Simple and rapid silver nanoparticles based antioxidant capacity assays: reactivity study for phenolic compounds. Food Chem 256:342–349. https://doi.org/10.1016/j.foodchem.2018.02.141
16. Amirjani A, Fatmehsari DH (2018) Colorimetric detection of ammonia using smartphones based on localized surface plasmon resonance of silver nanoparticles. Talanta 176:242–246. https://doi.org/10.1016/j.talanta.2017.08.022
17. Elahi N, Kamali M, Baghersad MH (2018) Recent biomedical applications of gold nanoparticles: a review. Talanta 184:537–556. https://doi.org/10.1016/j.talanta.2018.02.088
18. Xia Y, Si J, Li Z (2016) Fabrication techniques for microfluidic paper-based analytical devices and their applications for biological testing: a review. Biosens Bioelectron 77:774–789. https://doi.org/10.1016/j.bios.2015.10.032
19. He Y, Wu Y, Fu JZ, Bin WW (2015) Fabrication of paper-based microfluidic analysis devices: a review. RSC Adv 5:78109–78127. https://doi.org/10.1039/c5ra09188h
20. Tang N, Mu L, Qu H, Wang Y, Duan X, Reed MA (2017) Smartphone-enabled colorimetric trinitrotoluene detection using amine-trapped polydimethylsiloxane membranes. ACS Appl Mater Interfaces 9:14445–14452. https://doi.org/10.1021/acsami.7b03314
21. Piriya VSA, Joseph P, Daniel SCGK et al (2017) Colorimetric sensors for rapid detection of various analytes. Mater Sci Eng C 78:1231–1245. https://doi.org/10.1016/j.msec.2017.05.018
22. Jemmeli D, Marcoccio E, Moscone D, et al (2020) Highly sensitive paper-based electrochemical sensor for reagent free detection of bisphenol A. Talanta 216: https://doi.org/10.1016/j.talanta.2020.120924
23. Colozza N, Kehe K, Dionisi G, Popp T, Tsoutsoulopoulos A, Steinritz D, Moscone D, Arduini F (2019) A wearable origami-like paper-based electrochemical biosensor for sulfur mustard detection. Biosens Bioelectron 129:15–23. https://doi.org/10.1016/j.bios.2019.01.002
24. Hossain SMZ, Luckham RE, McFadden MJ, Brennan JD (2009) Reagentless bidirectional lateral flow bioactive paper sensors for detection of pesticides in beverage and food samples. Anal Chem 81:9055–9064. https://doi.org/10.1021/ac901714h
25. Luckham RE, Brennan JD (2010) Bioactive paper dipstick sensors for acetylcholinesterase inhibitors based on sol-gel/enzyme/gold nanoparticle composites. Analyst 135:2028–2035. https://doi.org/10.1039/c0an00283f
26. Badawy MEI, El-Aswad AF (2014) Bioactive paper sensor based on the acetylcholinesterase for the rapid detection of organophosphate and carbamate pesticides. Int J Anal Chem 2014: https://doi.org/10.1155/2014/536823, 2014, 1, 8
27. Kim HJ, Kim Y, Park SJ, Kwon C, Noh H (2018) Development of colorimetric paper sensor for pesticide detection using competitive-inhibiting reaction. Biochip J 12:326–331. https://doi.org/10.1007/s13206-018-2404-z
28. Wei Z, Li H, Wu J, Dong Y, Zhang H, Chen H, Ren C (2019) 3DRGO-NiFe2O4/NiO nanoparticles for fast and simple detection of organophosphorus pesticides. Chinese Chem Lett 31:177–180. https://doi.org/10.1016/j.cclet.2019.05.031
29. Chen H, Hu O, Fan Y, et al (2020) Fluorescence paper-based sensor for visual detection of carbamate pesticides in food based on CdTe quantum dot and nano ZnTPyP. Food Chem 327. https://doi.org/10.1016/j.foodchem.2020.127075
30. Nouanthavong S, Nacapricha D, Henry CS, Sameenoi Y (2016) Pesticide analysis using nanoceria-coated paper-based devices as a detection platform. Analyst 141:1837–1846. https://doi.org/10.1039/c5an02403j
31. Wang Q, Yin Q, Fan Y, Zhang L, Xu Y, Hu O, Guo X, Shi Q, Fu H, She Y (2019) Double quantum dots-nanoporphyrin fluorescence-

visualized paper-based sensors for detecting organophosphorus pesticides. Talanta 199:46–53. https://doi.org/10.1016/j.talanta.2019.02.023
32. Zhang Z, Ma X, Jia M, Li B, Rong J, Yang X (2019) Deposition of CdTe quantum dots on microfluidic paper chips for rapid fluorescence detection of pesticide 2,4-D. Analyst 144:1282–1291. https://doi.org/10.1039/c8an02051e
33. Liu W, Guo Y, Luo J, Kou J, Zheng H, Li B, Zhang Z (2015) A molecularly imprinted polymer based a lab-on-paper chemiluminescence device for the detection of dichlorvos. Spectrochim Acta - Part A Mol Biomol Spectrosc 141:51–57. https://doi.org/10.1016/j.saa.2015.01.020
34. Mei Q, Jing H, Li Y, Yisibashaer W, Chen J, Nan Li B, Zhang Y (2016) Smartphone based visual and quantitative assays on upconversional paper sensor. Biosens Bioelectron 75:427–432. https://doi.org/10.1016/j.bios.2015.08.054
35. Mandal S, Gole A, Lala N, Gonnade R, Ganvir V, Sastry M (2001) Studies on the reversible aggregation of cysteine-capped colloidal silver particles interconnected via hydrogen bonds. Langmuir 17:6262–6268. https://doi.org/10.1021/la010536d
36. Zare D, Akbarzadeh A, Barkhi M, Khoshnevisan K, Bararpour N, Noruzi M, Tabatabaei M (2012) L-arginine and L-glutamic acid capped gold nanoparticles at physiological PH: synthesis and characterization using agarose gel electrophoresis. Synth React Inorganic, Met Nano-Metal Chem 42:266–272. https://doi.org/10.1080/15533174.2011.609855
37. Taefi Z, Ghasemi F, Hormozi-Nezhad MR (2020) Selective colorimetric detection of pentaerythritol tetranitrate (PETN) using arginine-mediated aggregation of gold nanoparticles. Spectrochim Acta - Part A Mol Biomol Spectrosc 228. https://doi.org/10.1016/j.saa.2019.117803
38. Vanaraj S, Keerthana BB, Preethi K (2017) Biosynthesis, characterization of silver nanoparticles using quercetin from Clitoria ternatea L to enhance toxicity against bacterial biofilm. J Inorg Organomet Polym Mater 27:1412–1422. https://doi.org/10.1007/s10904-017-0595-8
39. Rawat KA, Kailasa SK (2014) Visual detection of arginine, histidine and lysine using quercetin-functionalized gold nanoparticles. Microchim Acta 181:1917–1929. https://doi.org/10.1007/s00604-014-1294-6
40. Stevanović M, Bračko I, Milenković M, Filipović N, Nunić J, Filipič M, Uskoković DP (2014) Multifunctional PLGA particles containing poly(l-glutamic acid)-capped silver nanoparticles and ascorbic acid with simultaneous antioxidative and prolonged antimicrobial activity. Acta Biomater 10:151–162. https://doi.org/10.1016/j.actbio.2013.08.030
41. Suvarna S, Das U, KC S et al (2017) Synthesis of a novel glucose capped gold nanoparticle as a better theranostic candidate. PLoS One 12:e0178202. https://doi.org/10.1371/journal.pone.0178202.g008
42. Dey R, Kar S, Joshi S, Maiti TK, Chakraborty S (2015) Ultra-low-cost 'paper-and-pencil' device for electrically controlled micromixing of analytes. Microfluid Nanofluidics 19:375–383. https://doi.org/10.1007/s10404-015-1567-3
43. Brereton RG (2003) Data analysis for the laboratory and chemical plant, 1st edn. Wiley
44. Zheng M, Wang Y, Wang C et al (2018) Green synthesis of carbon dots functionalized silver nanoparticles for the colorimetric detection of phoxim. Talanta 185:309–315. https://doi.org/10.1016/j.talanta.2018.03.066
45. Zeng S, Baillargeat D, Ho HP, Yong KT (2014) Nanomaterials enhanced surface plasmon resonance for biological and chemical sensing applications. Chem Soc Rev 43:3426–3452. https://doi.org/10.1039/c3cs60479a
46. Greenwood NN, Earnshaw A (1997) Chemistry of the elements, 2nd edn. Butterworth-Heinemann, Oxford
47. Heal HG (1980) The inorganic heterocyclic chemistry of sulfur, nitrogen, and phosphorus. AcademicPress, London